Layered Microporous Polymers by Solvent Knitting Method

Shaolei Wang [1], Chengxin Zhang [1], Yu Shu [1], Shulan Jiang [2], Qi Xia [2], Linjiang Chen [3], Shangbin Jin [1], Irshad Hussain [4], Andrew I. Cooper [3], Bien Tan [1]*

[1] Institute of Polymer Science and Engineering, School of Chemistry and Chemical Engineering, Huazhong University of Science and Technology, Luoyu Road No. 1037, Wuhan, 430074, China.
[2] State Key Laboratory of Digital Manufacturing Equipment and Technology, School of Mechanical Science and Engineering, Huazhong University of Science and Technology, Luoyu Road No. 1037, Wuhan, 430074, China.
[3] Department of Chemistry and Center for Materials Discovery, University of Liverpool, Crown Street, Liverpool L69 7ZD, United Kingdom.
[4] Department of Chemistry, SBA School of Science & Engineering (SSE), Lahore University of Management Sciences (LUMS), DHA, Lahore Cantt-54792, Lahore, Pakistan.
*Corresponding author. Email: bien.tan@mail.hust.edu.cn

Abstract

Two-dimensional (2D) nanomaterials especially 2D organic nanomaterials with unprecedentedly diverse and controlled structure, have attracted decent scientific interest. Among the prepartion strategies, "*top-down*" approach is a kind of considered low-cost and scalable strategies for obtain 2D organic nanomaterials. However, some factors of their layered counterparts limited the development and potential applications of 2D organic nanomaterials such as type, stability and strict synthetic conditions of layered counterparts. Herein we report, for the first time, a class of layered solvent knitting hypercrosslinked microporous polymers (SHCPs) prepared by improving *Friedel-Crafts* reaction and utilizing dichloroalkane as economical solvent, stable electrophilic reagent and external crosslinker at low temperature, which, more importantly, could be used as layered counterparts to obtain novel 2D SHCPs nanosheets by ultrasonic assisted solvent exfoliation method. This efficient and low-cost strategy can produce novel microporous organic polymers with layered structure, high surface area and gas storage capacity. The pore structure and surface area of these polymers can be controlled by tuning the chain length of solvent, the molar ratio of $AlCl_3$ and the size of monomers. Furthermore, we are the first to successfully obtain an unprecedentedly high surface area HCPs material (3002 $m^2 g^{-1}$), which shows decent gas storage capacity (4.82 mmol g^{-1} at 273 K and 1.00 bar for CO_2; 12.40 mmol g^{-1} at 77.3 K and 1.13 bar for H_2). This finding provides an opportunity for breaking the constraint of former knitting method and opening up avenues for the design and synthesis of novel layered HCPs materials.

Introduction

Graphene, being the first two-dimensional nanomaterials with atomic thickness, shows many intriguing properties including extreme mechanical strength and exceptionally high electronic and thermal conductivity (*1*), triggering enormous research interest in 2D nanomaterials (*2-9*). Unlike the graphene and 2D inorganic nanomaterials, single- or few-layered 2D organic nanomaterials possess unprecedented diverse and controlled structure by tailoring their building blocks and introducing functional groups, endowing themselves tunable properties, especially electronic and optoelectronic properties, and have also attracted decent scientific interest (*10-13*).

Inspired by the excellent properties and potential applications of 2D organic nanomaterials, two approaches i.e., "*bottom-up"* and "*top-down"* have been developed for their production. The on-surface polymerization is an important "*bottom-up*" strategy to obtain 2D organic nanomaterials by diverse organic reactions such as *Ullmann* coupling, boronic anhydridation reaction, acylation reactions, imine

formation *etc*. (*10-19*). Another "*bottom-up*" strategy i.e., topochemical polymerization such as air/water interface polymerization is also of great significance for obtaining large size 2D organic nanomaterials (*20-22*). The "*bottom-up*" synthetic strategy, however, is generally associated with challenges such as the requirement of ultrahigh vacuum, expensive substrates, specifically designed monomers, which impede their large-scale production and real applications in the field (*18, 20, 23*).

Numerous exfoliation attempts of layered bulk materials are defined as "*top-down*" approach, which is considered low-cost and scalable to produce 2D organic nanomaterials (*13, 24-26*). Due to the control over the geometry and proximity of the reactive sites of monomers, the prepared two-dimensional polymers crystals by single crystal approach can function as layered bulk materials to produce 2D organic nanomaterials (*26, 27*). Recently, combining the use of reversible reactions, solvothermal synthetic conditions and dynamic covalent chemistry, the covalent organic frameworks (COFs) with layered crystals and porosity have also been prepared and used as layered organic crystals (*28*). The direct exfoliation of bulk COFs also resulted in a series of the single-layered and even multi-layered 2D organic nanomaterials (*23, 29-32*). Compared with 2D polymer crystals, COFs possess many advantages of being low-cost and easier synthesis but their hydrothermal instability and high sensitivity to exfoliation limit their overall stability, development and potential applications in the field (*23, 28, 32*). It is, therefore, highly desirable to develop novel and cost-effective synthetic strategies to produce layered bulk materials with high hydrothermal stability.

Following the synthetic concept of COFs, the reversible bond formation is the key feature, which advances many other reversible reactions including *Friedel-Crafts* reactions feasible for the synthesis of layered structure synthetic materials (*33*). Recently, hypercrossliked polymers (HCPs) prepared by *Friedel-Crafts* alkylation based on strategies such as post-crosslinking of "*Davankov-type*" resins, self-polycondensation of multifunctional monomers and knitting aromatic compound polymers using external cross-linker, are receiving more interest due to their easier preparation, high chemical and thermal stability, low cost and sustainable mass production (*34, 35*). However, the open reaction system, high temperature and poor stability of carbocation intermediates as electrophilic reagents generally result in the production of amorphous HCPs materials. The development of efficient protocols for the synthesis of layered HCPs materials is, therefore, still a formidable scientific challenge.

Herein, we combine the development need for 2D organic nanomaterials with the scientific challenge of HCPs materials and propose a novel synthetic strategy to knit the first HCPs with layered structure, high surface area and gas uptake to produce 2D SHCPs nanosheets by ultrasonic assisted solvent exfoliation method. It resulted in great improvement in the *Friedel-Crafts* reaction conditions by introducing dichloroalkane as economical solvent, stable electrophilic reagent and external crosslinker, relatively less air-controlled environment, low temperature and gradient heating to control the rate of reaction of highly reactive carbocation intermediates. This process will overcome the constraint of previous knitting method and open up avenues for the design and synthesis of novel layered HCPs materials.

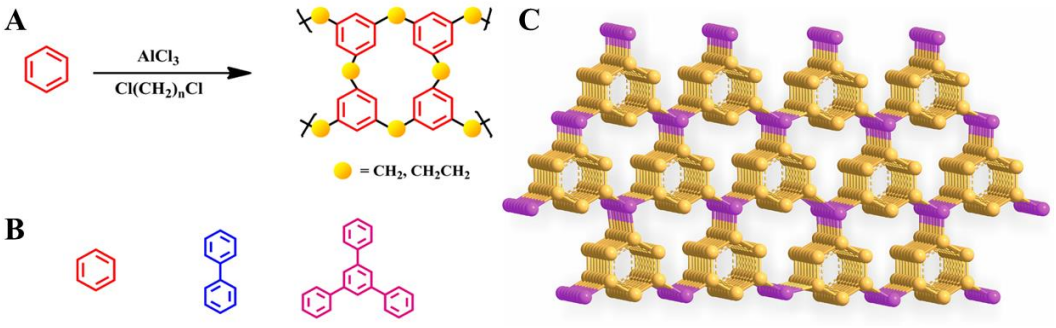

Scheme 1. Synthesis of polymers and building blocks structures and layered modelled structure of polymers. (A) The synthetic pathway to produce the network structure. **(B)** Molecular structures of building blocks for the network. **(C)** The layered model of benzene-based polymer.

Results

To the best of our knowledge, it is the first report that *Friedel-Crafts* alkylation reaction is used to produce HCPs with layered structure using dichloroalkane as an economical solvent (*34-36*). The HCPs show excellent thermal stability, high surface area and gas uptake, and also used as layered bulk materials to produce 2D SHCPs nanosheets by ultrasonic assisted solvent exfoliation method.

Structure Characterization and Simulation Calculation

To our pleasant surprise, the yield of polymers was very high, which is probably due to the favorable reaction of solvent with various aromatic precursors in the presence of $AlCl_3$ catalyst (*37, 38*). The Fourier transform infrared (FT-IR) spectroscopy confirms the existence of alkyl group in chemical structure of polymers by strong C-H stretching vibrations near 2920 cm^{-1} (**fig. S1-S7** and **table S1**). The ^{13}C cross-polarization/magic-angle spinning nuclear magnetic resonance (CP/MAS NMR) spectra of all these polymers, show resonance peaks near 140 and 133 ppm due to the substituted aromatic carbon and unsubstituted aromatic carbon respectively, and the resonance peaks near 37 ppm can be ascribed to the carbon of methylene linker (stemmed from dichloromethane as solvent and crosslinker) or ethylene linkers (stemmed from 1,2-dichloroethane as solvent and crosslinker) formed after *Friedel-Crafts* reaction (*39*) (**Fig. 1** and **fig. S8-S14**).

To further elucidate the mechanism of the polymerization process, we successfully isolated some dimers from initial stage of polymerization and characterized them by ^1H NMR and ^{13}C NMR, which clearly showed a resonance peak from methylene at about 4.10 ppm and 40 ppm and thus confirmed the formation of methylene linkage in the polymers (**fig. S15-S16**). Based on these analytical data, we believe that dichloroalkane is knitting the aromatic compounds to yield highly porous networks with methylene/ethylene as linkers under $AlCl_3$ catalysis, thus breaking the traditional cognitive of dichloroalkane as solvent for HCPs knitting strategies. Moreover, the low residual chlorine contents in methylene-based SHCP-3 (0.5 %) and ethylene-based SHCP-6 (0.01 %) and almost no catalyst residues in the polymers under ambient conditions suggest that the high yield of polymers is because of extensive crosslinking and incorporated abundant alkyl groups (**fig. S24**).

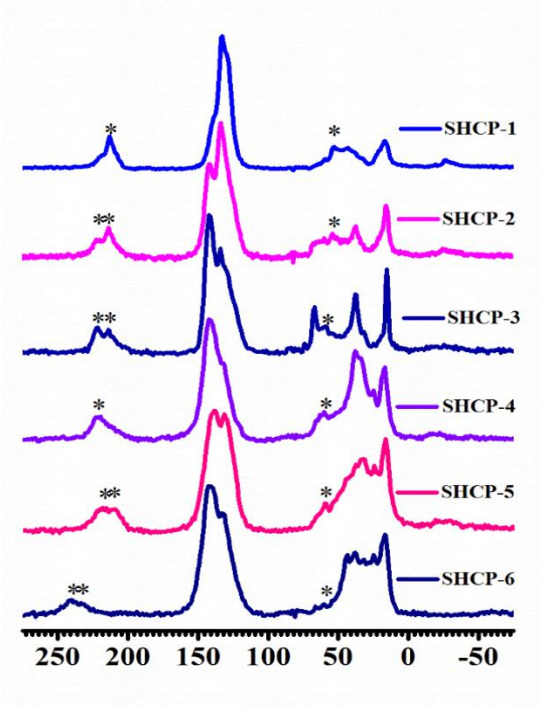

Fig. 1. NMR spectra of polymers. ^{13}C cross-polarization/magic-angle spinning (CP/MAS) NMR spectra of polymers; Asterisks denote spinning sidebands.

We further investigated the morphology and texture of polymers by field-emission scanning electron microscopy (FE-SEM) and high resolution transmission electron microscopy (HR-TEM). These polymers show block particles with layered structures, which are much different from the reported morphologies of HCPs (*39-41*) (**fig. S17-S23**). These polymers exhibited high thermal stability with thermal degradation up to 400 °C under nitrogen condition, and the residual weight of methylene-based polymers was more than that of ethylene-based polymers indicating their higher thermal stability (**fig. S24**).

The powder X-ray diffraction (PXRD) pattern of these novel polymers with layered structure showed a broad diffraction peak at 2θ = 23-27º (**fig. S25-S28**). Unlike the reported morphologies of HCPs (such as polymer 3), the SHCP-3 and SHCP-6 showed the obvious features of layered structures by HR-TEM and scanning transmission electron microscopy (STEM) at high resolution, confirming the existence of layered structures in these polymers (**Fig. 2** and **fig. S29**). We further evaluated the propensity of 1,3,5-triphenylbenzene (TPB), in its molecular form and in the form of oligomers (**fig. S30**), to form layered structures by calculating the energy required to create one unit of surface area relative to the bulk (details described in supporting information). Intrinsically, surfaces are less energetically favorable than the bulk of a material, and surfaces characterized by higher surface energies are expected to be present with smaller probabilities or to be less stable. Our calculations suggest that it is equally likely to form 2D slabs with the model TPB oligomers and with the TPB molecules. The surface energy is the same i.e., 0.10 J m^{-2} for both the amorphous packing of the TPB oligomers and the crystalline packing of the TPB molecules, as shown in **fig. S31** and **S32**, respectively. So, we assume that the layered structures might have been formed by the formation of chloroalkyl substituted aromatic monomers at low temperature, followed by their bridging and the formation of larger rings and finally knitting the layered structure at high temperature.

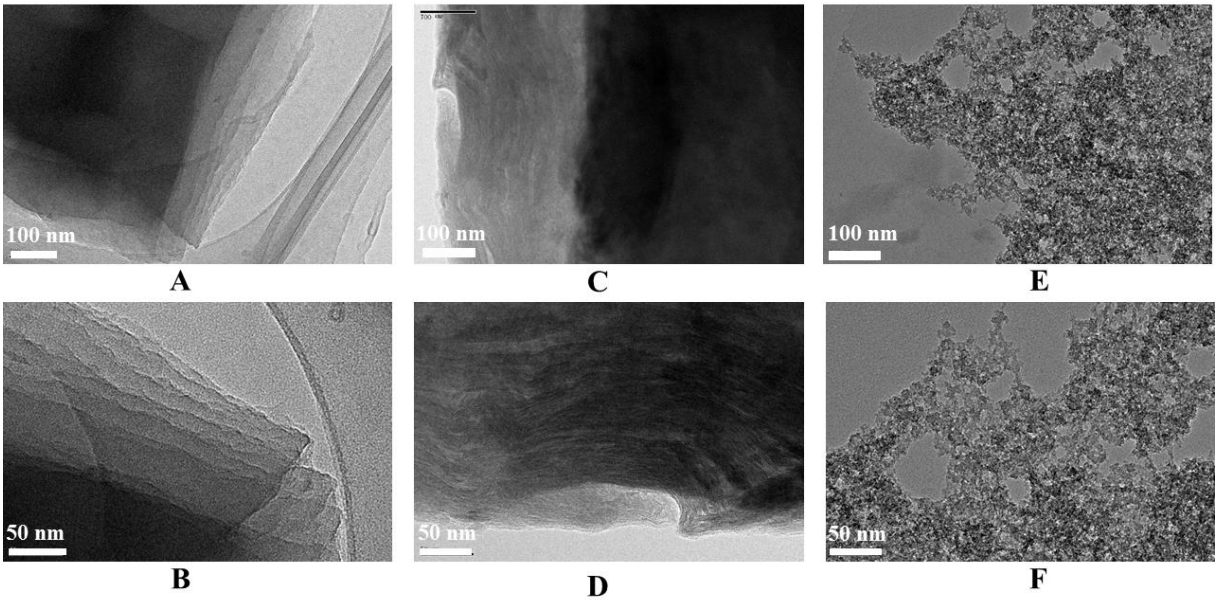

Fig. 2. HR-TEM data of SHCP-3, SHCP-6 and polymer 3. The HR-TEM images of SHCP-3 **(A, B)**, SHCP-6 **(C, D)** and polymer 3 **(E, F)** (knitted by formaldehyde dimethyl acetal (FDA) as external crosslinker) at different scale bar.

AFM Information of SHCPs Nanosheets

To further confirm the existence of layered nanosheet-like structures, we employed ultrasonic-assisted solvent exfoliation method to exfoliate bulk SHCP-3 and SHCP-6. The atomic force microscope (AFM) measurements further confirmed the precise information of SHCP-3 and SHCP-6 nanosheets. As shown in **Fig. 3**, the lateral dimensions of SHCP-3 nanosheets are fully consistent with its HR-TEM result and the height of SHCP-3 nanosheets varies from 2.0 nm to 50 nm (**fig. S33-S34**). Meanwhile, the nanosheets of SHCP-6 also show similar characteristics to nanosheets of SHCP-3, which suggests that all the SHCPs materials possess layered structure. The reproducibility of SHCPs nanosheets is remarkable by this exfoliation method. Moreover, the ionic liquids exfoliation also produce SHCPs nanosheets under ultrasonic conditions (*42*) (**fig. S34 C-34D**).

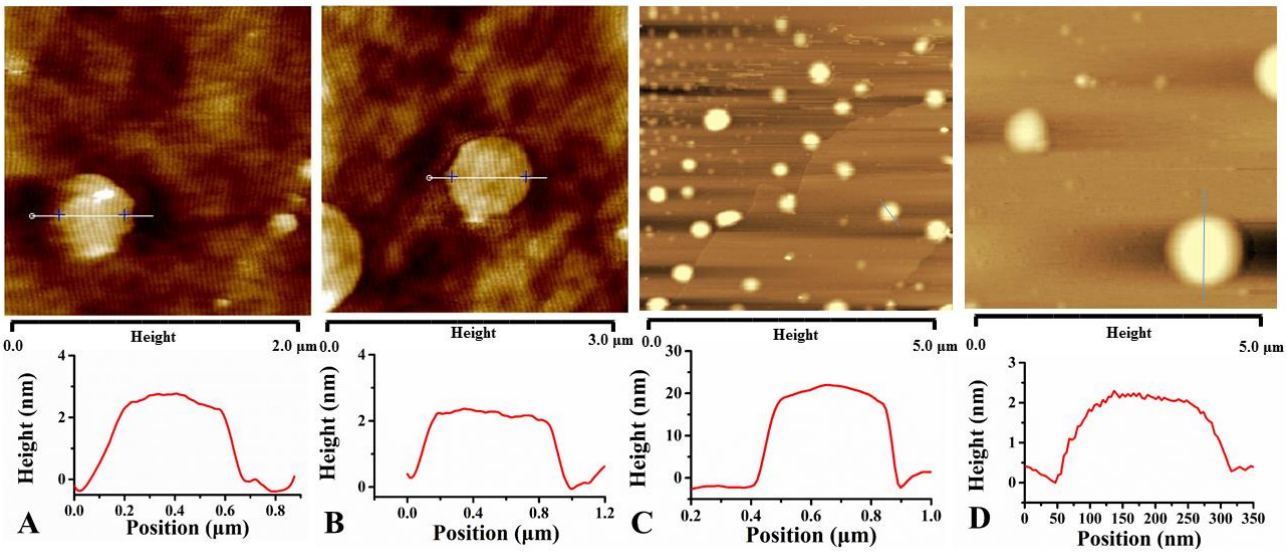

Fig. 3. AFM data of SHCP-3 and SHCP-6 nanosheets. (A, B) The AFM images and height analysis of SHCP-3 nanosheets on silicon wafer. **(C, D)** The AFM images and height analysis of SHCP-6 nanosheets on mica wafer.

Porosity of layered Microporous Polymers

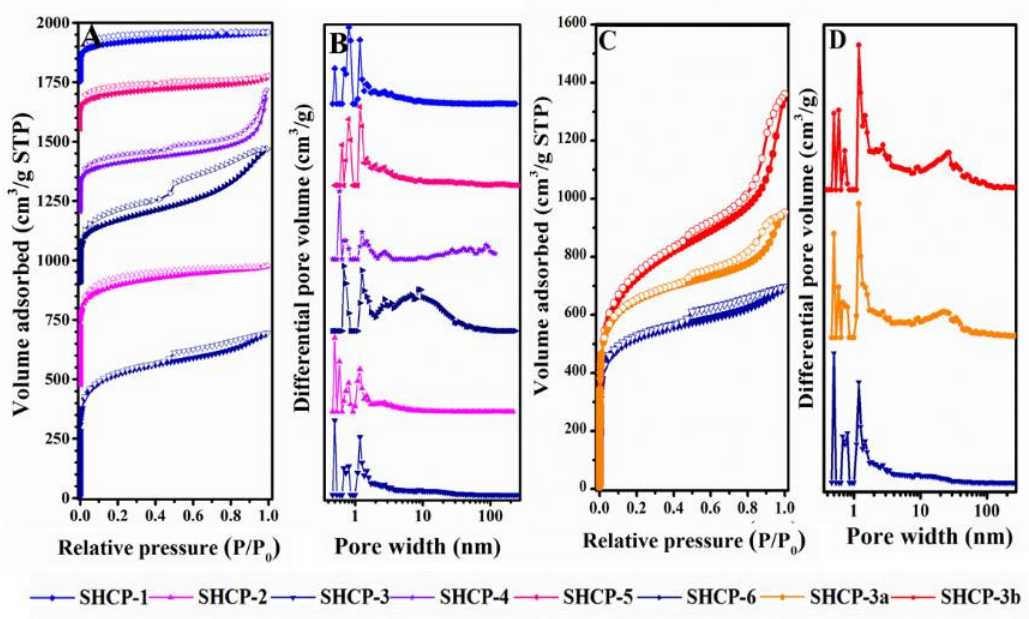

Fig. 4. Porosity data of polymers. (A, C) Nitrogen adsorption and desorption isotherms at 77.3 K; **(B, D)** pore distribution of pore size distribution calculated using DFT methods (slit pore models, differential pore volumes). Pore width of polymers.

Table 1. Composition and porosity of the polymers.

No.	Monomer	Solvent	S_{BET}* ($m^2 g^{-1}$)	S_L† ($m^2 g^{-1}$)	PV‡ ($cm^3 g^{-1}$)	MPV§ ($cm^3 g^{-1}$)
SHCP-1	Benzene	DCM	575	769	0.32	0.15
SHCP-2	Biphenyl	DCM	1475	1944	0.79	0.43
SHCP-3	1,3,5-triphenylbenzene	DCM	1808	2407	1.08	0.48
SHCP-4	Benzene	DCE	731	981	0.80	0.16
SHCP-5	Biphenyl	DCE	536	724	0.35	0.12
SHCP-6	1,3,5-triphenylbenzene	DCE	935	1281	0.88	0.15
SHCP-3a‖	1,3,5-triphenylbenzene	DCM	2525	3480	2.10	0.43
SHCP-3b¶	1,3,5-triphenylbenzene	DCM	3002	3896	2.33	0.42

* Surface area calculated from nitrogen adsorption isotherms at 77.3 K using BET equation. † Surface area calculated from nitrogen adsorption at 77.3 K using Langmuir equation. ‡ Pore volume calculated from nitrogen isotherm at P/P_0=0.995, 77.3 K. § Micropore volume calculated from the nitrogen isotherm at P/P_0=0.050. ‖ The amount of lewis acid is 12 molar ratio to 1,3,5-triphenyl benzene. ¶ The amount of Lewis acid is 24 molar ratio to 1,3,5-triphenylbenzene.

After confirming the chemical structure and layered structure of polymers, we further investigated the porosity parameters of polymers by nitrogen sorption analysis at 77.3 K. As shown in **Fig. 4A and 4C**, the isotherms of polymers exhibited a type I character with a steep nitrogen gas uptake at low relative

pressure ($P/P_0 < 0.001$), thus reflecting abundant microporous structure, and the existence of hysteresis for nitrogen sorption isotherm of polymers, suggest that polymers also possess mesopores (*43*, *44*). With an increase in the size of monomers, the BET surface area of polymers increased from 575 $m^2 g^{-1}$ to 1808 $m^2 g^{-1}$ for methylene-based polymers and from 731 $m^2 g^{-1}$ to 935 $m^2 g^{-1}$ for ethylene-based polymers, respectively (**Table 1**).

It is also worth mentioning that the surface area of methylene-based polymers increased remarkably and that of ethylene-based polymers decreased by increasing the molar ratio of $AlCl_3$ (**Table 1**, **table S2** and **Fig. 4C**). This result may be due to a faster rate of cross-linking and the low degree of free packing for building blocks leading to abundant mesopores and macropores, and much higher surface area for methylene-based polymers (**Fig. 4C**). The decrease in the microporosity of 1,3,5-triphenybenzene-based polymers from 44 % to 18 % also supports the proposed explanation (**Table 1**). However, the ethylene-based polymers with much higher yield have high ethylene content in their unit mass leading to more efficient packing and thus compromising the surface area. Most notably, SHCP-3b possesses abundant ultra-micropores (centered at 0.5 and 0.59 nm) and an extremely high specific surface area of 3002 $m^2 g^{-1}$, which is unprecedented in HCPs materials reported so far (*39*, *40*, *45-47*).

Based on the pore size distribution (PSD) analysis data, the chain length of solvent can effectively tune the pore size of polymers from 0.5 nm to 0.59 nm for benzene-based polymers, 0.64 nm for biphenyl-based polymers and 0.68 nm for 1,3,5-triphenylbenzene-based polymers. Moreover, the size of monomers can also be controlled to tune the pore size from 0.59 nm for SHCP-4 to 0.64 nm for SHCP-5 and to 0.68 nm for SHCP-6 (**Fig. 4B** and **table S3**). Therefore, this knitting method shows significant advantages including the systematic tuning of the porosity of layered structured HCPs by varying the chain length of solvent, the size of monomers and the molar ratio of $AlCl_3$.

Gas Uptake of layered Microporous Polymers

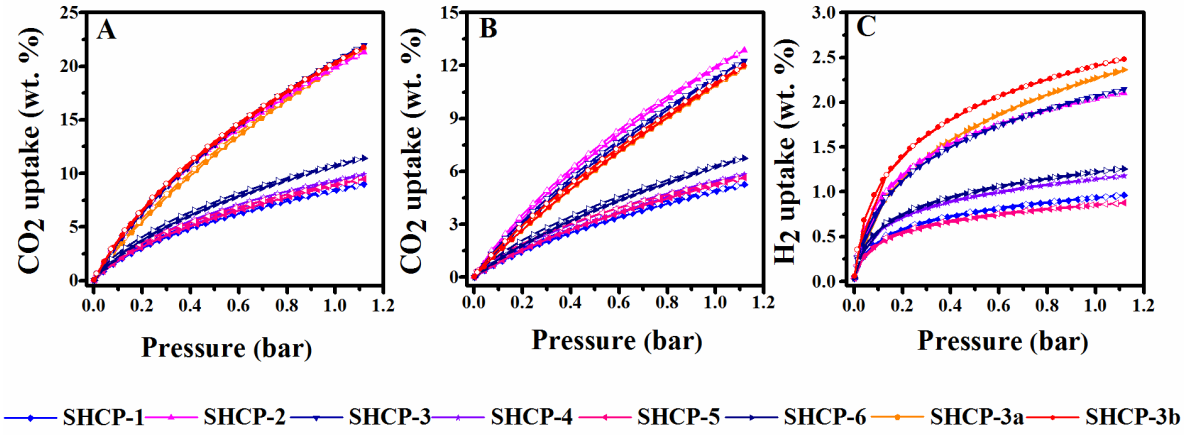

Fig. 5. Gas uptake data of polymers. (A) Volumetric CO_2 adsorption isotherms and desorption isotherms up to 1.00 bar at 273.15 K; **(B)** Volumetric CO_2 adsorption isotherms and desorption isotherms up to 1.00 bar at 298.15 K; **(C)** volumetric H_2 adsorption isotherms and desorption isotherms up to 1.13 bar at 77.3 K of polymers.

Table 2. Gas adsorption of the polymers.

No.	Monomer	Solvent	H_2 uptake* mmol g^{-1} (wt %)	CO_2 uptake† mmol g^{-1} (wt %)	CO_2 uptake‡ mmol g^{-1} (wt %)
SHCP-1	Benzene	DCM	4.80 (0.96)	1.95 (8.6)	1.14 (5.0)
SHCP-2	Biphenyl	DCM	10.55 (2.11)	4.64 (20.4)	2.77 (12.2)
SHCP-3	1,3,5-triphenyl benzene	DCM	10.70 (2.14)	4.84 (21.3)	2.64 (11.6)
SHCP-3a	1,3,5-triphenyl benzene	DCM	11.80 (2.36)	4.75 (20.9)	2.52 (11.1)
SHCP-3b	1,3,5-triphenyl benzene	DCM	12.40 (2.48)	4.82 (21.2)	2.57 (11.3)
SHCP-4	Benzene	DCE	5.90 (1.18)	2.11 (9.3)	1.23 (5.4)
SHCP-5	Biphenyl	DCE	4.40 (0.88)	2.02 (8.9)	1.18 (5.2)
SHCP-6	1,3,5-triphenyl benzene	DCE	6.30 (1.26)	2.43 (10.7)	1.43 (6.3)

* H_2 uptake determined volumetrically using a Micromeritics ASAP 2020 M analyzer at 1.13 bar and 77.3 K. † CO_2 uptake determined volumetrically using a Micromeritics ASAP 2020 M analyzer at 1.00 bar and 273.15 K. ‡ CO_2 uptake determined volumetrically using a Micromeritics ASAP 2020 M analyzer at 1.00 bar and 298.15 K.

The high specific surface area and abundant ultra-microporous nature of the polymers inspired us to investigate their gas uptake capacities. Based on the CO_2 isotherms of polymers, the CO_2 uptake of ethylene-based polymers is lower than that of methylene-based polymers (**Fig. 5A-5B** and **Table 2**) because of lower surface area and micropore volume (MPV) of ethylene-based polymers. Of these SHCPs polymers, SHCP-3 with much higher microporosity exhibits the highest CO_2 uptake of 4.84 mmol g^{-1} (273 K and 1.00 bar). The CO_2 uptake of SHCP-3 is, in fact, much higher than other HCPs materials under similar conditions such as 1,3,5-triphenylbenzene-based HCPs (3.61 mmol g^{-1}) (*39*), binaphthol-based HCPs (3.96 mmol g^{-1}) (*40*) and C1M1-Al (4.34 mmol g^{-1}) (*46*), possessing the highest CO_2 uptake capacity for HCPs materials reported so far.

Moreover, the CO_2 uptake capacity of SHCP-3 is comparable to that of the best reported porous materials such as CPOP-10 (S_{BET}: 3337 m^2 g^{-1}, less than 2.27 mmol g^{-1}, at 298 K and 1.00 bar) (*48-50*). Different from most of the porous materials with open metal-sites and CO_2-philic active sites such as heteroatoms and functional groups, the ultra-micropores of SHCP-3 may endow itself the outstanding CO_2 capture performance, which is comparable to the kinetic diameter of CO_2 to increase interactions between CO_2 and the pore walls (*51*). In addition, the CO_2 uptake of SHCP-2 with lower surface area is higher than that of SHCP-3 (298 K and 1.00 bar), which further proves the assumption that the ultra-micropores play a major role in the high CO_2 uptake of these SHCPs polymers.

Following the increasing environmental concerns and energy demand, porous materials are extensively being searched for the H_2 storage, therefore, we also set out to explore the potential of these polymers for H_2 uptake. As shown in **Fig. 5C**, all isotherms of polymers for H_2 adsorption are fully reversible, and exhibit a steep rise and unsaturation at low pressures. The methylene-based polymers exhibit higher H_2 uptake capacity than that of ethylene-based polymers. For example, the SHCP-3b showed the highest H_2 uptake up to 12.40 mmol g^{-1} (77.3 K and 1.13 bar), which, to the best of our knowledge, is also the highest H_2 uptake of HCPs materials reported to date (*39, 46*). The hydrogen

storage capacity of SHCP-3b is also higher than that of many reported MOPs under similar conditions (*28, 34, 52-54*), but slightly lower than that of the CPOP-1 (14 mmol g^{-1}) in MOP materials (*55*).

Discussion

In summary, this contribution demonstrated a solvent knitting strategy to produce layered hypercross-linked microporous polymers with high surface area and gas storage. This strategy has several outstanding characteristics: 1) the method can produce porous materials with high surface area, abundant micropore structure and high gas storage; 2) the simple synthesis conditions, the cheap reagents and high yield should allow economical and larger-scale production of such materials; 3) the tuneable porous structure and surface area by controlling the chain length of solvent, the molar ratio of $AlCl_3$ and the size of monomers can be achieved. Another merit of this strategy is the first ever demonstration of the formation of layered structure of HCPs materials. The very thin SHCP-3 nanosheets were obtained by ultrasonic-assisted solvent exfoliation method, which suggests this exfoliation method has the potential to form 2D nanosheets of other SHCPs. We are now trying to apply this strategy to develop new materials and explore intriguing properties and applications of this novel strategy by 'knitting' aromatic heterocyclic compounds (e.g., carbazole and thiophene), and functionalized large conjugated aromatic rings (e.g., graphene), and small aromatic molecular catalysts (e.g., porphyrin).

Materials and Methods

Materials. Benzene, biphenyl, $AlCl_3$ (anhydrous), $FeCl_3$ (anhydrous), ethanol, HCl, dichloromethane (DCM), 1, 2-dichloroethane (DCE) and N-Methyl pyrrolidone (NMP) were obtained from National Medicines Corporation Ltd. of China, all of which were of analytical grade and were used as received. 1, 3, 5-triphenylbenzene (syn-$PhPh_3$, Alfa Aesar, 98%), formaldehyde dimethyl acetal (FDA, Alfa Aesar, 98%) and 1-butyl-3-methylimidazolium bis (trifluoromethylsulfonyl)imide ([Bmim][Tf_2N], Alfa Aesar, 98%) was also used as received.

Synthesis of SHCP-1 (methylene-based polymer). Under a N_2 atmosphere, the catalyst ($AlCl_3$, 0.02 mol, 2.67 g) was added to a solution of benzene (0.78 g, 0.01 mol) in dichloromethane (DCM, 8 mL), and then the system connected nitrogen package to form relatively less air-controlled environment. The reaction system was then stirred at 0 °C for 4 h, 30 °C for 8 h, 40 °C for 12 h, 60 °C for 12 h and 80 °C for 24 h to obtain microporous polymer. The resulting precipitate was quenched using HCl-H_2O (v/v = 2:1), and washed thrice with water and twice with ethanol, extracted with ethanol for 48 h, and finally dried in a vacuum oven at 65 °C for 24 h. Yield = 134 %. Elemental analysis: C, 88.82; H, 5.94.

Synthesis of SHCP-1a (Methylene-based polymer). Following the synthesis conditions of SHCP-1, this SHCPs was produced by treating benzene (0.78 g, 0.01 mol) with $AlCl_3$ (0.04 mol, 5.33 g) in dichloromethane (DCM, 8 mL). Yield = 141 %.

Synthesis of SHCP-1b (Methylene-based polymer). Following the synthesis conditions of SHCP-1, this SHCPs was produced by treating benzene (0.78 g, 0.01 mol) with $AlCl_3$ (0.08 mol, 10.67 g) in dichloromethane (DCM, 8 mL). Yield = 147 %.

Synthesis of SHCP-2 (Methylene-based polymer). Following the synthesis conditions of SHCP-1, this SHCPs was produced by treating biphenyl (0.77 g, 0.005 mol) with $AlCl_3$ (0.02 mol, 2.67 g) in dichloromethane (DCM, 8 mL). Yield = 145 %. Elemental analysis: C, 86.24; H, 5.90.

Synthesis of SHCP-2a (Methylene-based polymer). Following the synthesis conditions of SHCP-1, this SHCPs was produced by treating biphenyl (0.77 g, 0.005 mol) with $AlCl_3$ (0.04 mol, 5.33 g) in dichloromethane (DCM, 8 mL). Yield = 149 %.

Synthesis of SHCP-2b (Methylene-based polymer). Following the synthesis conditions of SHCP-1, this SHCPs was produced by treating biphenyl (0.77 g, 0.005 mol) with $AlCl_3$ (0.08 mol, 10.67 g) in dichloromethane (DCM, 8 mL). Yield = 151 %.

Synthesis of SHCP-3 (Methylene-based polymer). Following the synthesis conditions of SHCP-1, this SHCPs was produced by treating *syn*-$PhPh_3$ (0.003 mol, 0.92 g) with $AlCl_3$ (0.018 mol, 2.40 g) in dichloromethane (DCM, 8 mL). Yield = 142 %. Elemental analysis: C, 85.74; H, 6.19; Cl, 0.5 %.

Synthesis of SHCP-3a (Methylene-based polymer). Following the synthesis conditions of SHCP-1, this SHCPs was produced by treating *syn*-$PhPh_3$ (0.003 mol, 0.92 g) with $AlCl_3$ (0.036 mol, 4.80 g) in dichloromethane (DCM, 8 mL). Yield = 146 %.

Synthesis of SHCP-3b (Methylene-based polymer). Following the synthesis conditions of SHCP-1, this SHCPs was produced by treating *syn*-$PhPh_3$ (0.003 mol, 0.92 g) with $AlCl_3$ (0.072 mol, 9.60 g) in dichloromethane (DCM, 8 mL). Yield = 151 %.

Synthesis of SHCP-4 (Ethylene-based polymer). Following the synthesis conditions of SHCP-1, this SHCPs was produced by treating benzene (0.78 g, 0.01 mol) with $AlCl_3$ (0.02 mol, 2.67 g) in 1,2-dichloroethane (DCE, 8 mL). Yield = 256 %. Elemental analysis: C, 86.66; H, 7.86.

Synthesis of SHCP-4a (Ethylene-based polymer). Following the synthesis conditions of SHCP-1, this SHCPs was produced by treating benzene (0.78 g, 0.01 mol) with $AlCl_3$ (0.04 mol, 5.33 g) in 1,2-dichloroethane (DCE, 8 mL). Yield = 284 %.

Synthesis of SHCP-4b (Ethylene-based polymer). Following the synthesis conditions of SHCP-1, this SHCPs was produced by treating benzene (0.78 g, 0.01 mol) with $AlCl_3$ (0.08 mol, 10.67 g) in 1,2-dichloroethane (DCE, 8 mL). Yield = 313 %.

Synthesis of SHCP-5 (Ethylene-based polymer). Following the synthesis conditions of SHCP-1, this SHCPs was produced by treating biphenyl (0.77 g, 0.005 mol) with $AlCl_3$ (0.02 mol, 2.67 g) in 1,2-dichloroethane (DCE, 8 mL). Yield = 265 %. Elemental analysis: C, 85.33; H, 7.08.

Synthesis of SHCP-5a (Ethylene-based polymer). Following the synthesis conditions of SHCP-1, this SHCPs was produced by treating biphenyl (0.77 g, 0.005 mol) with $AlCl_3$ (0.04 mol, 5.33 g) in 1,2-dichloroethane (DCE, 8 mL). Yield = 291 %.

Synthesis of SHCP-5b (Ethylene-based polymer). Following the synthesis conditions of SHCP-1, this SHCPs was produced by treating biphenyl (0.77 g, 0.005 mol) with $AlCl_3$ (0.08 mol, 10.67 g) in 1,2-dichloroethane (DCE, 8 mL). Yield = 322 %.

Synthesis of SHCP-6 (Ethylene-based polymer). Following the synthesis conditions of SHCP-1, this SHCPs was produced by treating *syn*-$PhPh_3$ (0.003 mol, 0.92 g) with $AlCl_3$ (0.018 mol, 2.40 g) in 1,2-dichloroethane (DCE, 8 mL). Yield = 279 %. Elemental analysis: C, 87.05; H, 7.00; Cl, 0.01 %.

Synthesis of SHCP-6a (Ethylene-based polymer). Following the synthesis conditions of SHCP-1, this SHCPs was produced by treating *syn*-$PhPh_3$ (0.003 mol, 0.92 g) with $AlCl_3$ (0.036 mol, 4.80 g) in 1,2-dichloroethane (DCE, 8 mL). Yield = 301 %.

Synthesis of SHCP-6b (Ethylene-based polymer). Following the synthesis conditions of SHCP-1, this SHCPs was produced by treating *syn*-$PhPh_3$ (0.003 mol, 0.92 g) with $AlCl_3$ (0.072 mol, 9.60 g) in 1,2-dichloroethane (DCE, 8 mL). Yield = 323 %.

Synthesis of polymer 3 (knitted by FDA as external crosslinker). Following the synthesis conditions of Reference **(***Macromolecules* **44**, 2410-2414 (2011)), this polymer 3 was produced by treating *syn*-$PhPh_3$ (0.005 mol, 1.53 g) with $FeCl_3$ (0.03 mol, 4.87 g) and FDA (0.03 mol, 2.28 g) in 1,2-dichloroethane (DCE, 10 mL).

Synthesis of 1,3,5-triphenylbenzene-based oligomer at 30 °C. Under a N_2 atmosphere, $AlCl_3$ (0.018 mol, 2.40 g) was added to a solution of *syn*-$PhPh_3$ (0.003 mol, 0.92 g) in dichloromethane (DCM, 8 mL), and then the system connected nitrogen package to form a relatively less air-controlled environment. The reaction system was then stirred at 0 °C for 4 h, 30 °C for 1 h, and then was quenched using HCl-H_2O (v/v = 2:1) and added 20 mL dichloromethane. The oil-water mixture was transferred to a 100 mL separating funnel and washed with abundant water until pH=7, and the oil phase was then dried by $MgSO_4$. The oligomer was obtained after removing the solvent and further purified by column chromatography.

The formula for polymeric yield.

$$w = \frac{m(polymers)}{m(monomers)} * 100\%$$

where $m_{polymers}$ is the weight of the dry polymers obtained by solvent knitting hypercrosslinked microporous polymers method, $m_{monomers}$ is the weight of the corresponding monomers of polymers.

The preparation of SHCPs nanosheets by ultrasonic assisted solvent exfoliation method.

Take the preparation of SHCP-3 nanosheets for example, using N-Methyl pyrrolidone (NMP) with high surface tensions as exfoliation solvent, 1 mg SHCP-3 was dispersed in 10 mL NMP and then sonicated with an ultrasonication bath (100 W) for 10 min. Thereafter, the resulting suspension was statically placed for four weeks and centrifuged at 5000 rpm for 10 min. Finally, the light yellow supernatant containing very thin 2D nanosheets was obtained, diluted by 10^5 times and deposited by drop-casting on silicon wafer surface (or mica wafer surface). The ionic liquids are also useful solvents to produce SHCPs nanosheets under ultrasonic conditions as demonstrated by Dai's group (*42*).

Characterization

FT-IR spectra were recorded on a Bruker Vertex 70 Spectrometer employing the KBr disk method. Solid-state ^{13}C cross-polarization/magic-angle spinning nuclear magnetic resonance (CP/MAS NMR) spectra were performed on a WB 400 MHz Bruker Avance II spectrometer. The ^{13}C CP/MAS NMR spectra were collected with a spinning rate of 8 kHz, and using a 4 mm double-resonance MAS probe. The ^{1}H and ^{13}C NMR spectra of oligomers for SHCP-3 were recorded by a Bruker AV400 spectrometer using $CDCl_3$ as solvent. Elemental analysis (EA) was performed on a Vario Micro cube Elemental Analyzer (Elementar, Germany), and the data of chlorine content of polymers was offered by Shanghai Institute of Organic Chemistry, Chinese Academy of Sciences. Thermogravimetric analysis (TGA) was performed from room temperature to 850 °C under nitrogen and air, employing a PerkinElmer Instrument Pyris1 TGA with a heating rate of 10 °C min^{-1}. The field-emission scanning electron microscopy (FE-SEM) images were recorded employing a FEI Sirion 200 field-emission scanning electron microscope operated at 10 kV. Before measurement, the samples were dried in a vacuum oven at 70 °C for 24 h and then sputter coated with platinum. Powder X-ray diffraction (PXRD) images were collected on X' Pert PRO with a scanning rate of 5^0 min^{-1}. The high resolution transmission electron microscopy (HR-TEM) images and scanning transmission electron microscopy (STEM) image of samples were recorded on a Tecnai G2 F30 microscope (FEI Corp. Holland). The thickness and size of nanosheets were carried out by Bruker Innova atomic force microscopy (AFM) in tapping mode. Before measurement, the diluted solution containing very thin nanosheets was deposited by drop-casting on the silicon wafer (or mica wafer) and dried in a vacuum oven at 80 °C for 72 h to allow to the complete evaporation of NMP. Gas (H_2, N_2, CO_2) sorption properties and specific surface area of samples were measured using a Micromeritics ASAP 2020 surface area and porosity analyzer. Before analysis, the samples were degassed at 110 °C for 8 h under vacuum of 10^{-5} bar. Pore size distribution was calculated

by N_2 adsorption isotherm employing the Tarazona nonlocal density functional theory (NLDFT) model assuming slit pore geometry. Total pore volumes (V_{toal}) were derived from nitrogen sorption isotherms at relative pressure P/P_0=0.995.

Surface energy calculation details

To obtain amorphous models for the TPB oligomers (Fig. 32), the Amorphous Cell module in BIOVIA Materials Studio 2016 was used, in conjunction with the COMPASS II force field. The orthorhombic simulation box for the bulk had the dimensions of 4.5 nm × 4.5 nm × 4.9 nm, while those of the box for the slab were 4.5 nm × 4.5 nm × 6.5 nm. The thickness of the slab at the narrowest cross-section was 2 nm. The atomistic bulk and slab models for the crystalline TPB were constructed based on the crystal structure reported in the Cambridge Structural Database (CCDC 867818). The simulation box for the crystalline slab was 4.7 nm × 4.5 nm × 4.0 nm, in which the slab thickness was 2 nm and the slab surfaces were the (1 0 0) plane of the bulk crystal.

All the atomistic models thus generated were further geometry-optimized with density functional based tight binding (DFTB) methods. DFTB in the self-consistent-charge parameterization was used in combination with a UFF dispersion correction (*56, 57*). Using these DFTB-optimized configurations, surface energies were determined using dispersion-corrected DFT. All DFT calculations made use of the Perdew–Burke–Ernzerhof (PBE) exchange–correlation functional with semi-empirical dispersion corrections from the DFT-D3 method (*58, 59*). The MOLOPT basis sets of the double-ζ quality were used, together with the Goedecker–Teter–Hutter pseudopotentials (*60-62*). The charge-density cutoff for the auxiliary plane-wave expansions was set to 350 Ry.

Surface energy calculations

We evaluated the propensity of 1,3,5-triphenylbenzene (TPB), in its molecular form and in the form of oligomers (Figure S30), to form layered structures, by calculating the energy required to create one unit of surface area relative to the bulk, or the surface energy, given as:

$$\gamma=(U_{slab}-U_{bulk})/2A$$

where $\boldsymbol{U_{slab}}$ is the total energy of the 2-dimonsional (2D) slab, at least 2 nm in thickness, with a minimum 2 nm vacuum region on each side, $\boldsymbol{U_{bulk}}$ is the total energy of the corresponding number of TPB units in bulk, and A is the surface area created on each side of the slab and is repeated periodically. Calculations were performed with first-principles density functional theory (DFT), using the CP2K package (https://www.cp2k.org).

Supplementary Materials

fig. S1. Fourier transform infrared (FT-IR) spectrum of SHCP-1.
fig. S2. Fourier transform infrared (FT-IR) spectrum of SHCP-2.
fig. S3. Fourier transform infrared (FT-IR) spectrum of SHCP-3.
fig. S4. Fourier transform infrared (FT-IR) spectrum of SHCP-3a.
fig. S5. Fourier transform infrared (FT-IR) spectrum of SHCP-4.
fig. S6. Fourier transform infrared (FT-IR) spectrum of SHCP-5.

References and Notes

1. A. K. Geim, Graphene: status and prospects. *Science* **324**, 1530-1534 (2009).
2. A. Pakdel, Y. Bando, D. Golberg, Nano boron nitride flatland. *Chem. Soc. Rev.* **43**, 934-959 (2014).
3. R. Ma, T. Sasaki, Nanosheets of oxides and hydroxides: ultimate 2D charge-bearing functional crystallites. *Adv. Mater.* **22**, 5082-5104 (2010).
4. N. Bilbao, I. Destoop, S. De Feyter, D. Gonzalez-Rodriguez, Two-dimensional nanoporous networks formed by liquid-to-solid transfer of hydrogen-bonded macrocycles built from DNA bases. *Angew. Chem. Int. Edit.* **55**, 659-663 (2016).
5. C. Tan, H. Zhang, Wet-chemical synthesis and applications of non-layer structured two-dimensional nanomaterials. *Nat. Commun.* **6**, (2015).
6. D. Chimene, D. L. Alge, A. K. Gaharwar, Two-dimensional nanomaterials for biomedical applications: emerging trends and future prospects. *Adv. Mater.* **27**, 7261-7284 (2015).
7. D. Deng, K. S. Novoselov, Q. Fu, N. Zheng, Z. Tian, X. Bao, Catalysis with two-dimensional materials and their heterostructures. *Nat. Nanotechnol.* **11**, 218-230 (2016).
8. Z. Liu, S. P. Lau, F. Yan, Functionalized graphene and other two-dimensional materials for photovoltaic devices: device design and processing. *Chem. Soc. Rev.* **44**, 5638-5679 (2015).
9. X. Zhuang, Y. Mai, D. Wu, F. Zhang, X. Feng, Two-dimensional soft nanomaterials: a fascinating world of materials. *Adv. Mater.* **27**, 403-427 (2015).
10. X.-H. Liu, C.-Z. Guan, D. Wang, L.-J. Wan, Graphene-like single-layered covalent organic frameworks: synthesis strategies and application prospects. *Adv. Mater.* **26**, 6912-6920 (2014).
11. J. Sakamoto, J. van Heijst, O. Lukin, A. D. Schlüter, Two-dimensional polymers: just a dream of synthetic chemists? *Angew. Chem. Int. Edit.* **48**, 1030-1069 (2009).
12. P. Payamyar, B. T. King, H. C. Oettinger, A. D. Schlueter, Two-dimensional polymers: concepts and perspectives. *Chem. Comm.* **52**, 18-34 (2016).
13. S.-L. Cai, W.-G. Zhang, R. N. Zuckermann, Z.-T. Li, X. Zhao, Y. Liu, The organic flatland recent advances in synthetic 2D organic layers. *Adv. Mater.* **27**, 5762-5770 (2015).
14. A. Gourdon, On-surface covalent coupling in ultrahigh vacuum. *Angew. Chem. Int. Edit.* **47**, 6950-6953 (2008).
15. H. Zhou, J. Liu, S. Du, L. Zhang, G. Li, Y. Zhang, B. Z. Tang, H.-J. Gao, Direct visualization of surface-assisted two-dimensional diyne polycyclotrimerization. *J. Am. Chem.Soc.* **136**, 5567-5570 (2014).
16. C.-Z. Guan, D. Wang, L.-J. Wan, Construction and repair of highly ordered 2D covalent networks by chemical equilibrium regulation. *Chem. Comm.* **48**, 2943-2945 (2012).
17. LafferentzL, EberhardtV, DriC, AfrichC, ComelliG, EschF, HechtS, GrillL, Controlling on-surface polymerization by hierarchical and substrate-directed growth. *Nat. Chem.* **4**, 215-220 (2012).
18. X.-H. Liu, C.-Z. Guan, S.-Y. Ding, W. Wang, H.-J. Yan, D. Wang, L.-J. Wan, On-surface synthesis of single-layered two-dimensional covalent organic frameworks via solid-vapor interface reactions. *J. Am. Chem. Soc.* **135**, 10470-10474 (2013).
19. F. Schlütter, F. Rossel, M. Kivala, V. Enkelmann, J.-P. Gisselbrecht, P. Ruffieux, R. Fasel, K. Müllen, π-Conjugated heterotriangulene macrocycles by solution and surface-supported synthesis toward honeycomb networks. *J. Am. Chem. Soc.* **135**, 4550-4557 (2013).
20. D. J. Murray, D. D. Patterson, P. Payamyar, R. Bhola, W. Song, M. Lackinger, A. D. Schlüter, B. T. King, Large area synthesis of a nanoporous two-dimensional polymer at the air/water interface. *J. Am. Chem. Soc.* **137**, 3450-3453 (2015).
21. P. Payamyar, K. Kaja, C. Ruiz-Vargas, A. Stemmer, D. J. Murray, C. J. Johnson, B. T. King, F. Schiffmann, J. Vandevondele, A. Renn, S. Gotzinger, P. Ceroni, A. Schutz, L. T. Lee, Z. Zheng, J.

Sakamoto, A. D. Schluter, Synthesis of a covalent monolayer sheet by photochemical anthracene dimerization at the air/water interface and its mechanical characterization by AFM indentation. *Adv. Mater.* **26**, 2052-2058 (2014).
22. W. Dai, F. Shao, J. Szczerbinski, R. McCaffrey, R. Zenobi, Y. Jin, A. D. Schlueter, W. Zhang, Synthesis of a two-dimensional covalent organic monolayer through dynamic imine chemistry at the air/water interface. *Angew. Chem. Int. Edit.* **55**, 213-217 (2016).
23. S. Chandra, S. Kandambeth, B. P. Biswal, B. Lukose, S. M. Kunjir, M. Chaudhary, R. Babarao, T. Heine, R. Banerjee, Chemically stable multilayered covalent organic nanosheets from covalent organic frameworks via mechanical delamination. *J. Am. Chem. Soc.* **135**, 17853-17861 (2013).
24. V. Nicolosi, M. Chhowalla, M. G. Kanatzidis, M. S. Strano, J. N. Coleman, Liquid exfoliation of layered materials. *Science* **340**, 1420-+ (2013).
25. A. Ciesielski, P. Samori, Graphene via sonication assisted liquid-phase exfoliation. *Chem. Soc. Rev.* **43**, 381-398 (2014).
26. M. J. Kory, M. Worle, T. Weber, P. Payamyar, S. W. van de Poll, J. Dshemuchadse, N. Trapp, A. D. Schluter, Gram-scale synthesis of two-dimensional polymer crystals and their structure analysis by X-ray diffraction. *Nat. Chem.* **6**, 779-784 (2014).
27. P. Kissel, R. Erni, W. B. Schweizer, M. D. Rossell, B. T. King, T. Bauer, S. Gotzinger, A. D. Schluter, J. Sakamoto, A two-dimensional polymer prepared by organic synthesis. *Nat. Chem.* **4**, 287-291 (2012).
28. S. Y. Ding, W. Wang, Covalent organic frameworks (COFs): from design to applications. *Chem. Soc. Rev.* **42**, 548-568 (2013).
29. I. Berlanga, R. Mas-Balleste, F. Zamora, Tuning delamination of layered covalent organic frameworks through structural design. *Chem. Comm.* **48**, 7976-7978 (2012).
30. I. Berlanga, M. L. Ruiz-Gonzalez, J. M. Gonzalez-Calbet, J. L. G. Fierro, R. Mas-Balleste, F. Zamora, Delamination of layered covalent organic frameworks. *Small* **7**, 1207-1211 (2011).
31. D. N. Bunck, W. R. Dichtel, Bulk synthesis of exfoliated two-dimensional polymers using hydrazone-linked covalent organic frameworks. *J. Am. Chem. Soc.* **135**, 14952-14955 (2013).
32. S. Mitra, S. Kandambeth, B. P. Biswal, A. M. Khayum, C. K. Choudhury, M. Mehta, G. Kaur, S. Banerjee, A. Prabhune, S. Verma, S. Roy, U. K. Kharu, R. Banerjee, Self-exfoliated guanidinium-based ionic covalent organic nanosheets (iCONs). *J. Am. Chem. Soc.* **138**, 2823-2828 (2016).
33. D. V. Nightingale, Alkylation and the action of aluminum halides on alkylbenzenes. *Chem. Rev.* **25**, 329-376 (1939).
34. S. J. Xu, Y. L. Luo, B. E. Tan, Recent development of hypercrosslinked microporous organic polymers. *Macromol. Rapid. Comm.* **34**, 471-484 (2013).
35. N. Fontanals, R. M. Marce, F. Borrull, P. A. G. Cormack, Hypercrosslinked materials: preparation, characterisation and applications. *Polym. Chem.* **6**, 7231-7244 (2015).
36. Z. A. Qiao, S. H. Chai, K. Nelson, Z. Bi, J. Chen, S. M. Mahurin, X. Zhu, S. Dai, Polymeric molecular sieve membranes via in situ cross-linking of non-porous polymer membrane templates. Nat. Commun. **5**, 3705 (2014).
37. A. P. Singh, A. K. Pandey, A novel catalytic method for the alkylation of benzene to diphenylmethane over H- ZSM- 5 zeolite catalysts. *Catal. Lett.* **60**, 157-159 (1999).
38. X. J. Cai, S. H. Cui, L. P. Qu, D. D. Yuan, B. Lu, Q. H. Cai, Alkylation of benzene and dichloromethane to diphenylmethane with acidic ionic liquids. *Catal. Commun.* **9**, 1173-1177 (2008).
39. B. Li, R. Gong, W. Wang, X. Huang, W. Zhang, H. Li, C. Hu, B. Tan, A new strategy to microporous polymers: knitting rigid aromatic building blocks by external cross-linker. *Macromolecules* **44**, 2410-2414 (2011).
40. R. Dawson, L. A. Stevens, T. C. Drage, C. E. Snape, M. W. Smith, D. J. Adams, A. I. Cooper, Impact of water coadsorption for carbon dioxide capture in microporous polymer sorbents. *J. Am.*

Chem. Soc. **134**, 10741-10744 (2012).
41. J. Zhang, Z.-A. Qiao, S. M. Mahurin, X. Jiang, S.-H. Chai, H. Lu, K. Nelson, S. Dai, Hypercrosslinked phenolic polymers with well-developed mesoporous frameworks. *Angew. Chem. Int. Edit.* **54**, 4582-4586 (2015).
42. X. Wang, P. F. Fulvio, G. A. Baker, G. M. Veith, R. R. Unocic, S. M. Mahurin, M. Chi, S. Dai, Direct exfoliation of natural graphite into micrometre size few layers graphene sheets using ionic liquids. Chem. Commun. **46**, 4487-4489 (2010).
43. K. S. W. Sing., D. H. Everett, R. A. W. Haul, L. Moscou, P. A. Pierotti, J. Rouquerol, T. Siemieniewska, Reporting physisorption data for gas/solid systems with special reference to the determination of surface area and porosity. *Pure. Appl. Chem.* **57**, 603-619 (1985).
44. M. Thommes, K. Kaneko, A. V. Neimark, J. P. Olivier, F. Rodriguez-Reinoso, J. Rouquerol, K. S. W. Sing, Physisorption of gases, with special reference to the evaluation of surface area and pore size distribution. *Pure. Appl. Chem.* **87**, 1051-1069 (2015).
45. S. W. Yao, X. Yang, M. Yu, Y. H. Zhang, J. X. Jiang, High surface area hypercrosslinked microporous organic polymer networks based on tetraphenylethylene for CO2 capture. *J. Mater. Chem. A* **2**, 8054-8059 (2014).
46. G. Liu, Y. Wang, C. Shen, Z. Ju, D. Yuan, A facile synthesis of microporous organic polymers for efficient gas storage and separation. *J. Mater. Chem. A* **3**, 3051-3058 (2015).
47. M. Seo, S. Kim, J. Oh, S.-J. Kim, M. A. Hillmyer, Hierarchically porous polymers from hyper-cross-linked block polymer precursors. *J. Am. Chem. Soc.* **137**, 600-603 (2015).
48. J. Y. Wang, L. Huang, R. Y. Yang, Z. Zhang, J. W. Wu, Y. S. Gao, Q. Wang, D. O'Hare, Z. Y. Zhong, Recent advances in solid sorbents for CO2 capture and new development trends. *Energy. Environ. Sci.* **7**, 3478-3518 (2014).
49. Z. Xiang, R. Mercado, J. M. Huck, H. Wang, Z. Guo, W. Wang, D. Cao, M. Haranczyk, B. Smit, Systematic tuning and multifunctionalization of covalent organic polymers for enhanced carbon capture. *J. Am. Chem. Soc.* **137**, 13301-13307 (2015).
50. K. J. Msayib, N. B. McKeown, Inexpensive polyphenylene network polymers with enhanced microporosity. *J. Mater. Chem. A* **4**, 10110-10113 (2016).
51. R. Dawson, A. I. Cooper, D. J. Adams, Chemical functionalization strategies for carbon dioxide capture in microporous organic polymers. *Polym. Int.* **62**, 345-352 (2013).
52. N. B. McKeown, P. M. Budd, Polymers of intrinsic microporosity (PIMs): organic materials for membrane separations, heterogeneous catalysis and hydrogen storage. *Chem. Soc. Rev.* **35**, 675-683 (2006).
53. Y. H. Xu, S. B. Jin, H. Xu, A. Nagai, D. L. Jiang, Conjugated microporous polymers: design, synthesis and application. *Chem. Soc. Rev.* **42**, 8012-8031 (2013).
54. M. G. Rabbani, H. M. El-Kaderi, Synthesis and characterization of porous benzimidazole-linked polymers and their performance in small gas storage and selective uptake. *Chem. Mater.* **24**, 1511-1517 (2012).
55. Q. Chen, M. Luo, P. Hammershøj, D. Zhou, Y. Han, B. W. Laursen, C.-G. Yan, B.-H. Han, Microporous polycarbazole with high specific surface area for gas storage and separation. *J. Am. Chem. Soc.* **134**, 6084-6087 (2012).
56. M. Elstner, D. Porezag, G. Jungnickel, J. Elsner, M. Haugk, T. Frauenheim, S. Suhai, G. Seifert, Self-consistent-charge density-functional tight-binding method for simulations of complex materials properties. *Phys. Rev. B* **58**, 7260-7268 (1998).
57. L. Zhechkov, T. Heine, S. Patchkovskii, G. Seifert, H. A. Duarte, An efficient a Posteriori treatment for dispersion interaction in density-functional-based tight binding. *J. Chem. Theory. Comput.* **1**, 841-847 (2005).
58. J. P. Perdew, K. Burke, M. Ernzerhof, Generalized gradient approximation made simple. *Phys. Rev. Lett.* **78**, 1396-1396 (1997).
59. S. Grimme, J. Antony, S. Ehrlich, H. Krieg, A consistent and accurate ab initio parametrization of

density functional dispersion correction (DFT-D) for the 94 elements H-Pu. *J. Chem. Phys.* **132**, (2010).
60. J. VandeVondele, J. Hutter, Gaussian basis sets for accurate calculations on molecular systems in gas and condensed phases. *J. Chem. Phys.* **127**, (2007).
61. C. Hartwigsen, S. Goedecker, J. Hutter, Relativistic separable dual-space Gaussian pseudopotentials from H to Rn. *Phys. Rev. B* **58**, 3641-3662 (1998).
62. M. Krack, Pseudopotentials for H to Kr optimized for gradient-corrected exchange-correlation functionals. *Theor. Chem. Acc.* **114**, 145-152 (2005).

Acknowledgments

We thank the Analysis and Testing Center, Huazhong University of Science and Technology for characterization assistance in characterization of materials. **Fundding:** This work was financially supported by the program for National Natural Science Foundation of China (No. 21474033/51273074/51173058). **Author contributions:** B.T. conceived the project and supervised the experiment. S.W., C.Z. and Y.S. synthesized and characterized the SHCPs. Q.X. and S.J. did the AFM measurement. L.C. performed the simulation and caculation of layered strcture. A.C., S.J. and I.H., in addition to technical and intellectual discussion/contribution, helped in writing/improving the manuscript. S.W. and B.T. co-wrote the manuscript. **Competing interests:** The authors declare that they have no competing financial interests. **Data and materials availability:** All data need to evaluate the conclusion in the paper are present in the paper and/or the supplemently materials. Additional data related to this paper may be requested from the authors.

Figures and Tables

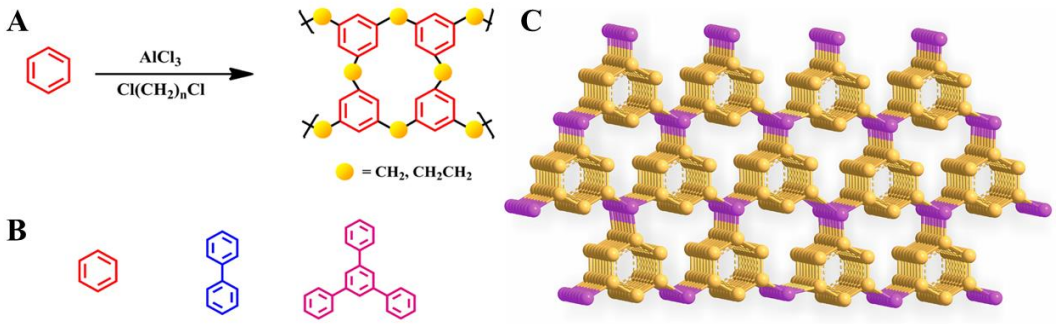

Scheme 1. Synthesis of polymers and building blocks structures and layered modelled structure of polymers. (A) The synthetic pathway to produce the network structure. **(B)** molecular structures of building blocks for the network. **(C)** The layered model of benzene-based polymer.

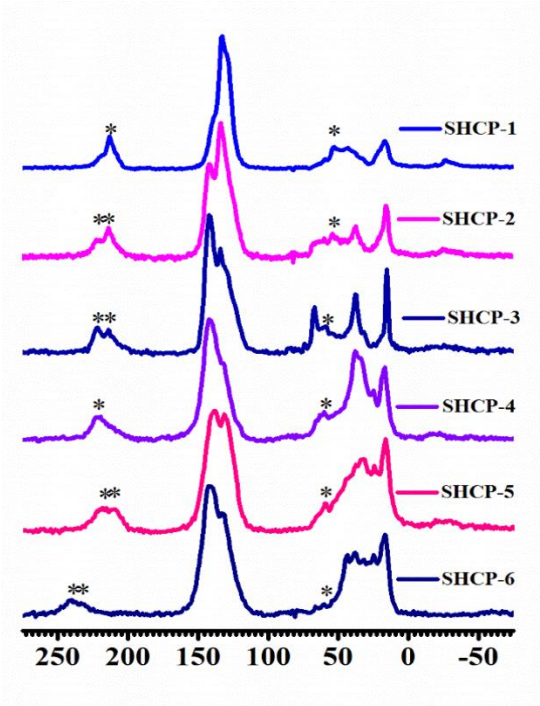

Fig. 1. NMR spectra of polymers. ^{13}C cross-polarization/magic-angle spinning (CP/MAS) NMR spectra of polymers; Asterisks denote spinning sidebands.

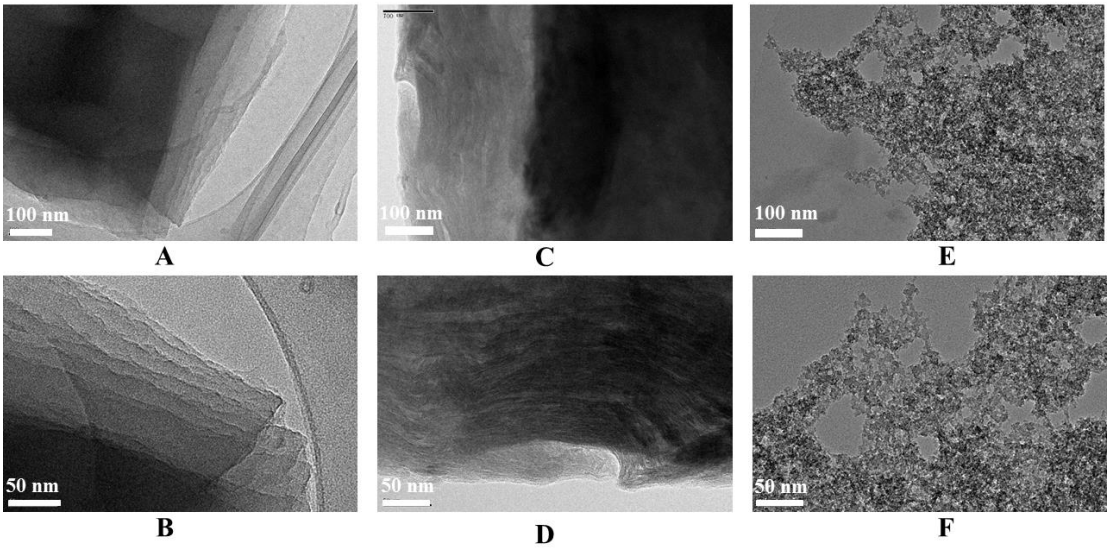

Fig. 2. HR-TEM data of SHCP-3, SHCP-6 and polymer 3. The HR-TEM images of SHCP-3 **(A, B)**, SHCP-6 **(C, D)** and polymer 3 **(E, F)** (knitted by formaldehyde dimethyl acetal (FDA) as external crosslinker) at different scale bar.

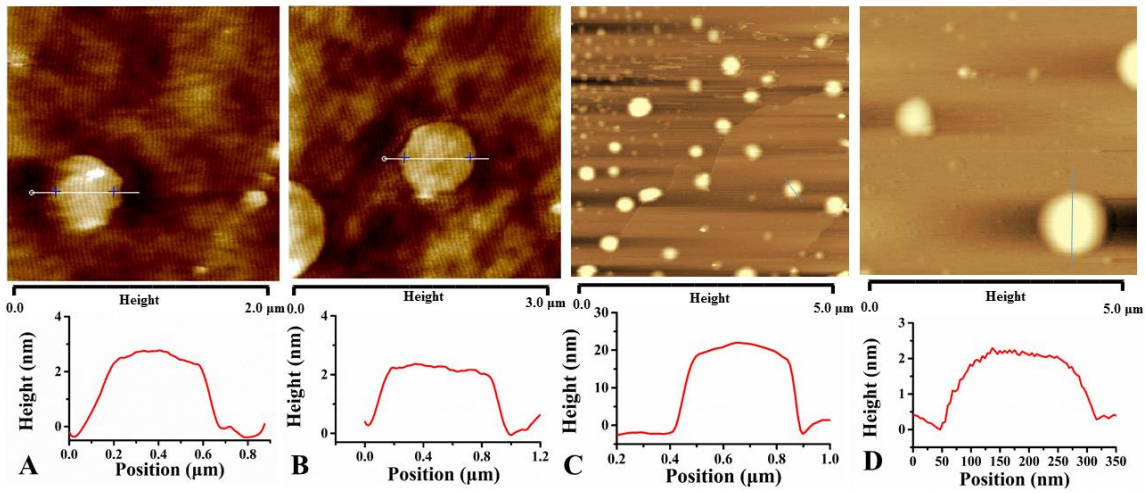

Fig. 3. AFM data of SHCP-3 and SHCP-6 nanosheets. (A, B) The AFM images and height analysis of SHCP-3 nanosheets on silicon wafer. **(C, D)** The AFM images and height analysis of SHCP-6 nanosheets on mica wafer.

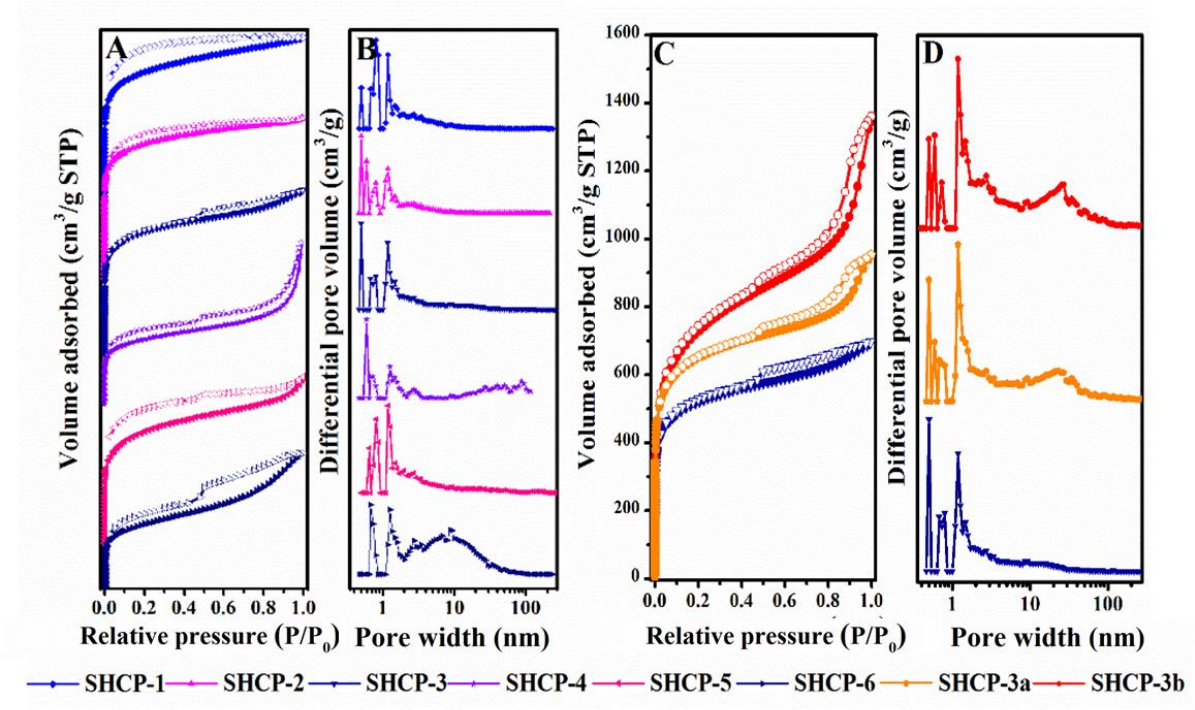

Fig. 4. Porosity data of polymers. (A, C) Nitrogen adsorption and desorption isotherms at 77.3 K; **(B, D)** pore distribution of pore size distribution calculated using DFT methods (slit pore models, differential pore volumes). Pore width of polymers.

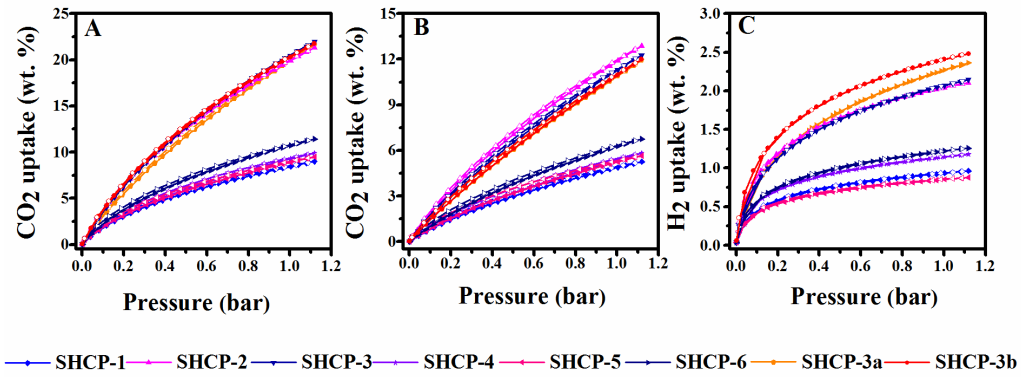

Fig. 5. Gas uptake data of polymers. (A) Volumetric CO_2 adsorption isotherms and desorption isotherms up to 1.00 bar at 273.15 K; **(B)** Volumetric CO_2 adsorption isotherms and desorption isotherms up to 1.00 bar at 298.15 K; **(C)** volumetric H_2 adsorption isotherms and desorption isotherms up to 1.13 bar at 77.3 K of polymers.

Table 1. Composition and porosity of the polymers.

No.	Monomer	Solvent	S_{BET}* ($m^2\ g^{-1}$)	S_L† ($m^2\ g^{-1}$)	PV‡ ($cm^3\ g^{-1}$)	MPV§ ($cm^3\ g^{-1}$)
SHCP-1	Benzene	DCM	575	769	0.32	0.15
SHCP-2	Biphenyl	DCM	1475	1944	0.79	0.43
SHCP-3	1,3,5-triphenylbenzene	DCM	1808	2407	1.08	0.48
SHCP-4	Benzene	DCE	731	981	0.80	0.16
SHCP-5	Biphenyl	DCE	536	724	0.35	0.12
SHCP-6	1,3,5-triphenylbenzene	DCE	935	1281	0.88	0.15
SHCP-3a‖	1,3,5-triphenylbenzene	DCM	2525	3480	2.10	0.43
SHCP-3b¶	1,3,5-triphenylbenzene	DCM	3002	3896	2.33	0.42

* Surface area calculated from nitrogen adsorption isotherms at 77.3 K using BET equation. † Surface area calculated from nitrogen adsorption at 77.3 K using Langmuir equation. ‡ Pore volume calculated from nitrogen isotherm at P/P_0=0.995, 77.3 K. § Micropore volume calculated from the nitrogen isotherm at P/P_0=0.050. ‖ The amount of lewis acid is 12 molar ratio to 1,3,5-triphenyl benzene. ¶ The amount of Lewis acid is 24 molar ratio to 1,3,5-triphenylbenzene.

Table 2. Gas adsorption of the polymers.

No.	Monomer	Solvent	H_2 uptake* mmol g^{-1} (wt %)	CO_2 uptake† mmol g^{-1} (wt %)	CO_2 uptake‡ mmol g^{-1} (wt %)
SHCP-1	Benzene	DCM	4.80 (0.96)	1.95 (8.6)	1.14 (5.0)
SHCP-2	Biphenyl	DCM	10.55 (2.11)	4.64 (20.4)	2.77 (12.2)
SHCP-3	1,3,5-triphenyl benzene	DCM	10.70 (2.14)	4.84 (21.3)	2.64 (11.6)
SHCP-3a	1,3,5-triphenyl benzene	DCM	11.80 (2.36)	4.75 (20.9)	2.52 (11.1)
SHCP-3b	1,3,5-triphenyl benzene	DCM	12.40 (2.48)	4.82 (21.2)	2.57 (11.3)
SHCP-4	Benzene	DCE	5.90 (1.18)	2.11 (9.3)	1.23 (5.4)
SHCP-5	Biphenyl	DCE	4.40 (0.88)	2.02 (8.9)	1.18 (5.2)
SHCP-6	1,3,5-triphenyl benzene	DCE	6.30 (1.26)	2.43 (10.7)	1.43 (6.3)

* H_2 uptake determined volumetrically using a Micromeritics ASAP 2020 M analyzer at 1.13 bar and 77.3 K. † CO_2 uptake determined volumetrically using a Micromeritics ASAP 2020 M analyzer at 1.00 bar and 273.15 K. ‡ CO_2 uptake determined volumetrically using a Micromeritics ASAP 2020 M analyzer at 1.00 bar and 298.15 K.

TOC